Research Article Vol. 5, No. 11 / November 2018 / Optica 1418

Compressive characterization of telecom photon pairs in the spatial and spectral degrees of freedom

Nicola Montaut,[1,†] Omar S. Magaña-Loaiza,[2,3,*,†] Tim J. Bartley,[1] Varun B. Verma,[2] Sae Woo Nam,[2] Richard P. Mirin,[2] Christine Silberhorn,[1] and Thomas Gerrits[2]

[1]Integrated Quantum Optics, Universität Paderborn, Warburger Strasse 100, 33098 Paderborn, Germany
[2]National Institute for Standards and Technology, 325 Broadway, Boulder, Colorado 80305, USA
[3]Department of Physics and Astronomy, Louisiana State University, Baton Rouge, Louisiana 70803, USA
*Corresponding author: maganaloaiza@lsu.edu

Received 11 June 2018; revised 26 September 2018; accepted 10 October 2018 (Doc. ID 334816); published 6 November 2018

In the past few years, physicists and engineers have demonstrated the possibility of utilizing multiple degrees of freedom of the photon to perform information processing tasks for a wide variety of applications. Furthermore, complex states of light offer the possibility of encoding and processing many bits of information in a single photon. However, the challenges involved in the process of extracting large amounts of information, encoded in photonic states, impose practical limitations to realistic quantum technologies. Here, we demonstrate characterization of quantum correlated photon pairs in the spatial and spectral degrees of freedom. Our technique utilizes a series of random projective measurements in the spatial basis that do not perturb the spectral properties of the photon. The sparsity in the spatial properties of downconverted photons allows us to exploit the potential of compressive sensing to reduce the number of measurements to reconstruct spatial and spectral properties of correlated photon pairs at telecom wavelength. We demonstrate characterization of a photonic state with 12×10^9 dimensions using only 20% of the measurements with respect to the conventional raster scan technique. Our characterization technique opens the possibility of increasing and exploiting the complexity and dimensionality of quantum protocols that utilize multiple degrees of freedom of light with high efficiency.

https://doi.org/10.1364/OPTICA.5.001418

1. INTRODUCTION

Recent research in quantum information processing has been triggered by the possibility of utilizing multiple degrees of the photon to prepare high-dimensional states [1–4]. The construction of interesting Hilbert spaces has been demonstrated by engineering complex photonic superpositions in time, frequency, position, transverse momentum, angular position, and orbital angular momentum [1–6]. Interestingly, the transverse spatial degree of freedom has offered a flexible platform to test complex quantum information protocols in a relatively simple fashion. For example, quantum high-dimensional protocols have been implemented by defining Hilbert spaces in the pixel basis [2,7–10]. In general, photons entangled in these representative degrees of freedom have been utilized to perform quantum metrology, quantum imaging, quantum communication, and quantum simulations [1,2,5,6,11].

The characterization of quantum-correlated photons in these degrees of freedom has been demonstrated over the last decade [5,6,12–15]. Typically, these states are characterized by implementing a series of projective measurements on each of the correlated photons. It is worth noting that the number of measurements scales quadratically with the dimension size of the state [7,16]. This imposes severe practical limitations, for example, in the information that one can decode from high-dimensional states. Recent proposals demonstrated to alleviate this limitation by utilizing optimization algorithms such as compressive sensing (CS). These techniques allow for the estimation of approximate states that describe photonic systems with only a small fraction of the total required measurements [7,13,16–18].

CS can play an important role in photonic quantum technologies and low-light level applications. Examples include single-photon level imaging, entanglement characterization, and quantum state and process tomography [7,13,15,16,18–24]. CS provides an alternative to single-photon detector arrays, permitting one to reduce operational overhead in systems employing raster scanning [25,26]. This technique has been crucial in demonstrating entanglement imaging, measurement of spatial wave functions, and characterizing high-dimensional entangled states in the variables of position and momentum [7,13,19–24].

In this work, we utilize CS to demonstrate a proof-of-principle characterization of the spatial and spectral properties of quantum-correlated photon pairs produced through a process of spontaneous parametric downconversion (SPDC). We utilize a digital micromirror device (DMD) to project the spatial profile of downconverted photon pairs onto a series of random matrices. The transmitted photons are then sent to a fiber spectrometer that

allows one to map the spectral content of the photons to time bins [27–29]. Our high efficiency, low-jitter superconducting nanowire single-photon detectors (SNSPDs) allow us to measure joint-spectral information of the correlated photons while we reconstruct spatial information [30]. In our experiment, the spatial and spectral degrees of freedom define complex high-dimensional states that contain approximately 12×10^9 elements. We characterize these states with only 20% of the measurements required in conventional measurement techniques that use pixel-by-pixel raster scan. The significant reduction in the number of measurements required to characterize sources of SPDC make our technique a powerful diagnostic tool for photonic quantum technologies.

2. THEORETICAL ANALYSIS

The process of SPDC produces photons correlated in various degrees of freedom. In this work, we aim to characterize the spatial and spectral degrees of freedom. These properties of our photons define a high-dimensional Hilbert space described by the following state:

$$|\Psi\rangle = \sum_{\omega=1}^{D_\omega} f_\omega |\omega\rangle_s |\omega\rangle_i \otimes \sum_{j=1}^{D_j} s_j |x_j\rangle_s |x_j\rangle_i, \tag{1}$$

where f_ω represents the probability amplitude of finding signal and idler in the frequency mode $|\omega\rangle_{s,i}$. Similarly, the spatial degree of freedom is described by a coherent superposition of spatial ("pixel") states $|x_j\rangle_{s,i}$; the probability of finding a photon pair in these states is described by the coefficient s_j.

In our experiment, we implement a series of projective measurements in the spatial and spectral degrees of freedom described by the operator $\hat{A}$. The operator $\hat{A}$ is defined by the tensor product of the operator $\hat{T}$ and the operator $\hat{O}$ that act on the spectral and spatial degrees of freedom, respectively:

$$|\Phi\rangle = \hat{A}|\Psi\rangle = \sum_{\omega=1}^{D_\omega} \hat{T} f_\omega |\omega\rangle_s |\omega\rangle_i \otimes \sum_{j=1}^{D_j} \hat{O} s_j |x_j\rangle_s |x_j\rangle_i. \tag{2}$$

The operator $\hat{T}$ maps the spectral components of the downconverted photons to times of arrival, whereas the operator $\hat{O}$ projects the spatial profile of signal and idler photons onto m random patterns described by $\hat{O}_{m,l}$, where l represents a pixel index:

$$|\Phi\rangle = \sum_{t=1}^{D_t} \hat{f}_t |t\rangle_s |t\rangle_i \otimes \sum_{j=1}^{D_j} \sum_{l} \hat{O}_{m,l} s_j |x_l\rangle_s |x_l\rangle_i. \tag{3}$$

We can recast the equation above in the form $\hat{\Phi} = \hat{A}\hat{\Psi}$, which can be expressed as

$$\begin{pmatrix} \phi_1 \\ \phi_2 \\ \vdots \\ \phi_M \end{pmatrix} = \begin{pmatrix} A_{1,1} & A_{1,2} & \dots & A_{1,N} \\ A_{2,1} & A_{2,2} & \dots & A_{2,N} \\ \vdots & \vdots & \ddots & \vdots \\ A_{M,1} & A_{M,2} & \dots & A_{M,N} \end{pmatrix} \begin{pmatrix} \psi_1 \\ \psi_2 \\ \vdots \\ \psi_N \end{pmatrix}. \tag{4}$$

It is possible to implement the matrix $\hat{A}$ to measure the total elements in $\hat{\Phi}$; subsequently, this information can be used to invert Eq. (4) and determine the target state $\hat{\Psi}$. In this case, the elements in the matrix $\hat{A}$ define the dimensionality of our measuring device [10]. However, we take advantage of the sparsity in the target state by using optimization techniques [26]. This allows us to estimate the state $\hat{\Psi}$ with only a small fraction of measurements. We do this by minimizing the quantity below:

$$\min_{\Psi'} \sum_l \|\nabla \Psi'_l\|_{\ell_1} + \frac{\mu}{2} \|\hat{A}\hat{\Psi}' - \hat{\Phi}\|^2_{\ell_2}. \tag{5}$$

Here, $\nabla \Psi'_l$ is the discrete gradient of Ψ' at position x_l, and μ is a regularization term. The optimal value of μ should be chosen considering the specific characteristics of the state $\hat{\Psi}$ and the amount of noise in our data [26]. The solution of the optimization problem in Eq. (5), through CS, allows us to estimate the state $|\Psi'\rangle$ that is an approximation of $|\Psi\rangle$.

3. EXPERIMENTAL SETUP

The outline of our experimental setup is depicted in Fig. 1. We use a 785 nm, 76 MHz pulse-picked to 3.64 MHz Ti:Sapphire laser to pump a rubidium exchanged, periodically poled potassium titanyl phosphate (Rb:PPKTP) waveguide (length = 8 mm, poling period = 46.1 μm), that produces correlated photon pairs at telecom wavelengths [31]. Our type-II Rb:PPKTP waveguide produces photons with orthogonal polarizations. The generated downconverted photons illuminate a DMD that is used to measure their spatial properties. We utilize a folded 4-f imaging system to compensate for the dispersion caused by the DMD (not shown). The downconverted photon pairs are then separated by a polarizing beam splitter (PBS) and coupled into long single-mode fibers. We used low-jitter SNSPDs with an efficiency of approximately 85% to detect correlated photon pairs [30].

The DMD has an array of 1024×768 micromirrors that are individually controlled. We generate a sequence of random patterns by changing the states of the pixels on the DMD. The "on" pixels reflect light to the optical path of the setup, whereas the "off" state directs away from the optical path. We project a series of sensing matrices onto the DMD. Each projective measurement picks fragments of information from the spatial mode of the photons. We use the information collected from all projective measurements and by solving the optimization problem in Eq. (5) through total variation of augmented Lagrangian alternating

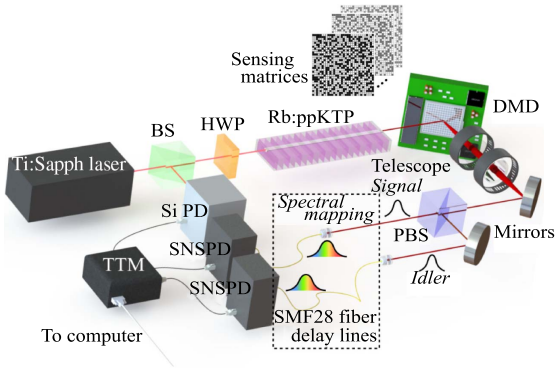

Fig. 1. Experimental setup. Photon pairs at telecom wavelength ($\lambda_{SPDC} = 1570$ nm) are generated in a Rb:PPKTP waveguide through a type II SPDC process. The spatial reconstruction is performed by probing the signal and idler photons using a DMD displaying a series of random patterns. Reflected photons are then imaged with a telescope and spatially separated by a PBS. We simultaneously obtain spatial and spectral information by using 10 km of fiber that allows us to map frequency to time. Finally, we utilize SNSPDs and a fast TTM to detect photons and record times of arrival. A small portion of the pump is separated by a beam splitter and detected by a fast photodiode. We use the signal from the photodiode to trigger our TTM, which is used to count downconverted photons.

direction algorithm (TVAL3) [26] to estimate approximations of the spatial distributions of SPDC photons.

4. CHARACTERIZATION OF PHOTON PAIRS IN THE SPATIAL DOMAIN

We show the reconstructed spatial distributions of signal and idler photons in Figs. 2(a) and 2(b). These results were obtained by performing a series of projective measurements with matrices containing 64×64 elements. We use a sampling ratio of 20% and an integration time of 4 s. The average number of accumulated counts per frame for the signal mode is 545,172 and 543,326 for the idler mode. The signal-to-noise ratios for the signal and idler modes are 27.1 and 18.5, respectively. The reconstruction of each spatial profile took 1 s in a standard personal computer. The slight displacement of the reconstructed modes along the vertical axis is due to the imperfect polishing on the face of the waveguide. As a result, the signal and idler photons experience different effective refractive indices that cause a small spatial displacement between them [see Figs. 2(a) and 2(b)].

Recently, there has been a strong impetus to employ discrete pixel basis in high-dimensional quantum protocols [2,7–10]. This photonic degree of freedom has been utilized in the context of quantum state engineering, quantum state tomography, and information processing [2,7,8]. For example, pixel entanglement was utilized to generate qudits [9]; this idea was further extended by Dixon and co-workers, who demonstrated information encoding in high-dimensional entangled states defined in the pixel basis [2]. In these cases, the Hilbert space is defined by the spatial resolution of the pixels in the spatial light modulator or DMD [7,10,13]. Thus, the spatial characterization of telecom photons shown in Fig. 2 can have important implications for quantum information protocols that utilize the spatial degree of freedom of photons [2,7,8,10].

5. SPATIAL AND SPECTRAL CHARACTERIZATION OF PHOTON PAIRS

We use the pixels on the DMD to discretize the spatial degree of freedom of SPDC photons. It has been demonstrated that the amount of information that can be encoded in a single photon scales with the dimensionality of the state [32]. Consequently, high-dimensional photonic states represent important information resources. We estimate the spatial dimensionality of a quantum state projected on the DMD by assessing the number of pixels occupied by each reconstructed mode. In this work, we have determined the dimensionality by considering only the illuminated region on the DMD rather than the dimensionality of our measurement device given by the matrix $\hat{A}$. We estimate the spatial dimensions of the quantum state by using the $1/e^2$ diameter of each reconstructed mode [17]. Thus, the dimensionality of the signal (s) and idler (i) states are estimated to be $\mathcal{N}_s = 40 \times 40$ and $\mathcal{N}_i = 43 \times 43$ spatial bins, respectively. These states define the joint spatial distribution, which provides a measure of correlations between the photon pairs. The dimensionality of the joint spatial probability distribution is estimated to be $\mathcal{N}_{\mathrm{JSD}} = \mathcal{N}_s \times \mathcal{N}_i = 2.96 \times 10^6$. The joint spatial distribution is depicted in Fig. 2(c), which is mapped out by plotting coincidences between signal and idler modes.

We also characterize the spectral information of our SPDC source by implementing a fiber-based time-of-flight spectrometer [27,28]. As shown in Fig. 1, the experimental setup comprises long single-mode telecom fibers that act as a dispersive medium to stretch and translate the spectrum of the downconverted photons to time-of-arrival [29]. The photon's time-of-arrival is accurately recorded with a fast time tagging module (TTM) and low-jitter SNSPDs. The spectral resolution of this measurement depends on the detector jitter (≈120 ps) and the amount of dispersion, which is determined by the length of the fibers (10 km). The total dispersion introduced by each fiber is ≈170 ps nm^{-1} at wavelengths around 1570 nm. Therefore, the spectral resolution of our measurement apparatus is $\delta\lambda \approx 0.7$ nm.

The joint arrival time of SPDC photons is shown in Fig. 3(a). The marginals are estimated by taking the transfer function of the arrival time of the downconverted photons. The resulting spectra of both photons are shown in Fig. 3(b). The nonlinear crystal is designed to show a phase-matching peak at 1570 nm, which corresponds to the main peak in the spectrum. Hence, the photon bandwidths are estimated by selecting only the arrival time tags corresponding to this peak, as shown in the inset of Fig. 3(b). The spectral $1/e^2$ bandwidth of the measured signal and idler photons are 26 and 43 nm, respectively.

We observe noise contributions from shorter wavelengths; see low-intensity satellite peaks at $\lambda_s \approx 1414$ nm and $\lambda_i \approx 1515$ nm. Since the waveguide is multimode for the pump field, we speculate that the sharp peak at $\lambda_s = 1414$ nm is generated from a higher-order pump spatial mode, which triggers a parasitic SPDC process [33]. On the other hand, the broader peak at $\lambda_i = 1515$ nm arises from optical Cherenkov radiation that is phase-matched in our waveguide [34]. This process occurs when short pump pulses are transmitted through an electro-optic medium (here, PPKTP waveguide), which induces a nonlinear polarization

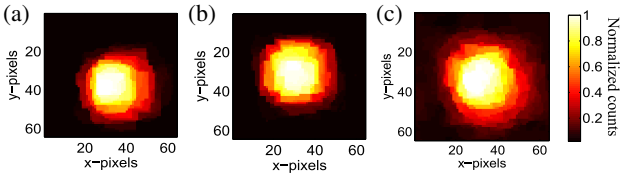

Fig. 2. Spatial profile of (a) signal and (b) idler reconstructed using a sampling ratio of 20%. The sensing matrix contains $\mathcal{N} = 64 \times 64 = 4096$ elements. (c) shows the reconstructed joint spatial distribution obtained through coincidences between signal and idler photons.

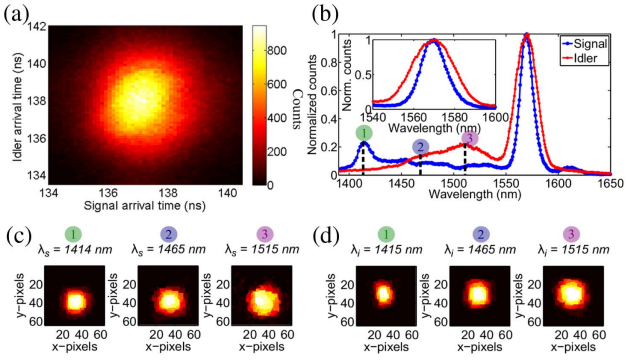

Fig. 3. (a) Joint photon arrival time. (b) Full marginal spectra of signal and idler photons with phase matching peak at 1570 nm (inset). (c) and (d) Reconstructed spatial profiles for signal and idler photons for shorter wavelengths generated due to a slightly multimode pump spectrum.

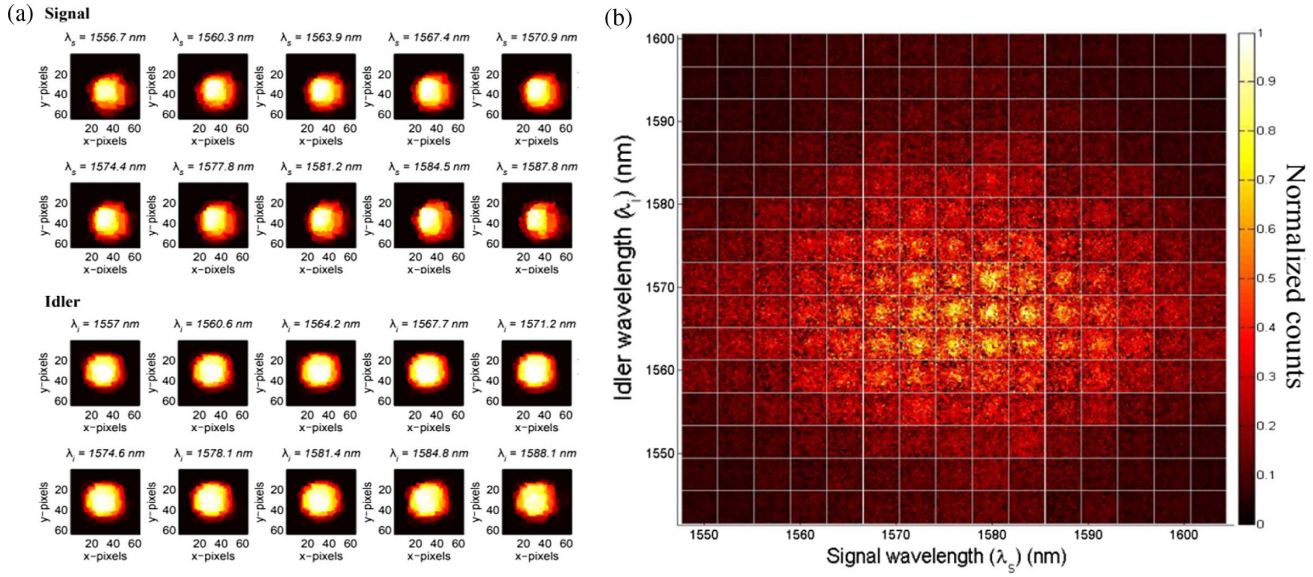

Fig. 4. (a) Spatiospectral reconstructions of signal and idler photons. These marginal distributions are obtained within the main phase-matched peak using a sampling ratio of 20% and sensing matrices with 64 × 64 pixels. (b) The joint spectral intensity distributions are plotted by spectrally resolving the coincidences between the signal and idler photons into 15 bins, each within its respective bandwidths of the main phase-matched peak. Each frame on the plot corresponds to a spatial reconstruction on a 64 × 64 sensing array. This is obtained by integrating over the coincidences measured within individual spectral bins. The integration time required per pattern of the CS measurement was set to 4 s.

that radiates in a Cherenkov-like cone along the propagation direction of the pump pulse [35]. To obtain qualitative understanding of these parasitic modes, we reconstruct the spatial distributions of signal and idler photons within this wavelength range. We plot in Figs. 3(c) and 3(d) the outcome of the reconstructions at both satellite peaks and at an intermediate wavelength to demonstrate a trend in the signal and idler. The geometric distortion observed in the spatial profiles shown in Fig. 3 is a consequence of lateral chromatic aberration [36]. This is due to refraction effects that affect different wavelength components differently. In our experiment, the collimation lens induces an increase in the size of spatial modes with large spectral detuning. This kind of color distortion is typically corrected through algorithms based on the implementation of digital filters [37].

Our experimental apparatus offers the possibility of identifying sources of distinguishability in SPDC photons. This represents an important problem that severely affects the visibility of quantum protocols that rely on quantum interference. The generation of nondegenerate photons through SPDC processes, the lateral displacements originated by imperfect polishing, or tilted surfaces in nonlinear crystals are ubiquitous problems that can be easily identified through our technique. The possibility of characterizing both the spatial and spectral degrees of freedom allows one to decode significant amounts of information encoded in single photons [2,6,7,13,14,38]. For this reason, we demonstrate characterization of our source by resolving spatial features as a function of spectrum. In Fig. 4(a), we show reconstructions within the main phase-matching peak of the signal and idler photons performed with a 20% sampling ratio. Joint spectral distributions are shown in Fig. 4(b). Our ability to spectrally resolve changes of the order of $\delta\lambda \approx 0.7$ nm allows us to define high-dimensional states with a dimension of $\mathcal{S}_s = 54$ for signal and $\mathcal{S}_i = 60$ for idler. The resolution of the fiber spectrometer is also experimentally estimated from the wavelength difference between two consecutive spectral bins to be $\delta\lambda = (0.70 \pm 0.05)$ nm. The dimensionality ($\mathcal{D}$) of the measured quantum state in the spatiospectral domain is estimated to be $\mathcal{D}_s = 40 \times 40 \times 54$ and $\mathcal{D}_i = 43 \times 43 \times 60$ for signal and idler photons, respectively. The joint spatiospectral distribution of the reconstructed states is therefore estimated to be $\mathcal{D}_{\mathrm{JSSD}} = \mathcal{D}_s \times \mathcal{D}_i = 11.98 \times 10^9$ dimensions. This dimensionality is smaller than the one defined by our measuring device.

Our experimental results demonstrate the potential of CS to characterize sources of SPDC and thus high-dimensional photonic states. However, due to the inherent low-photon flux in most quantum optics experiments, we investigate the robustness of our technique by characterizing a bulk PPKTP source that produces correlated photons at a rate of 6000 photons per second. We quantify the fidelity of our reconstructions as a function of sampling ratio. The full measurement scan that represents a sampling ratio of 100% is taken as the target state (ψ_T). The accuracy of the spatial reconstruction is estimated by calculating the fidelity (see Fig. 5) of the retrieved states (ψ_R) as a function of sampling ratio. This is defined as $\mathcal{F} = |\langle\psi_R|\psi_T\rangle|^2$. The error on the fidelity in Fig. 5 is determined using Monte Carlo simulations on a sample size of (100 signal × 100 idler) matrices, generated using a

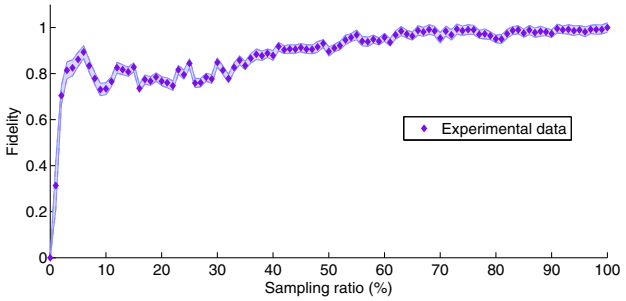

Fig. 5. Fidelity of the reconstructed high-dimensional state as a function of number of measurements.

Poissonian error distribution on the detected signal and idler counts. Remarkably, the main features of the photon modes are retrieved with sampling ratios close to 20% and beyond this, only a slight improvement is observed in the reconstructed profiles.

6. CONCLUSIONS

We demonstrate an efficient characterization of telecom photon pairs entangled in the spatial and spectral degrees of freedom. We utilize CS and a fiber-based spectrometer to reduce the number of measurements required to characterize high-dimensional states with billions of elements. The complex photonic states that we measured in this work would require unfeasibly large acquisition times with other conventional techniques. The dramatic reduction in the number of measurements required to characterize sources of SPDC makes our technique a powerful diagnostic tool for quantum protocols that exploit multiple degrees of freedom of light. Last but not least, the simplicity and robustness of our technique enables the identification of experimental conditions that limit the performance of quantum protocols that rely on efficient quantum interference; as such, we anticipate the use of our scheme in laboratories for optical quantum technologies.

Funding. FP7 People: Marie-Curie Actions (PEOPLE) (ITN PIQUE 608062); Gottfried Wilhelm Leibniz-Preis Program; Deutsche Forschungsgemeinschaft (DFG) (1115/4-1).

Acknowledgment. We acknowledge Travis Autry and Josue Davila-Rodriguez for helpful discussions.

†These authors contributed equally to this work.

REFERENCES

1. Z. Xie, T. Zhong, S. Shrestha, J. C. Bienfang, A. Restelli, F. N. C. Wong, and C. W. Wong, "Harnessing high dimensional hyper entanglement through a biphoton frequency comb," Nat. Photonics **9**, 536–542 (2015).
2. P. B. Dixon, G. A. Howland, J. Schneeloch, and J. C. Howell, "Quantum mutual information capacity for high dimensional entangled states," Phys. Rev. Lett. **108**, 143603 (2012).
3. T. Zhong, H. Zhou, R. D. Horansky, C. Lee, V. B. Verma, A. E. Lita, A. Restelli, J. C. Bienfang, and F. N. C. Wong, "Photon-efficient quantum key distribution using time-energy entanglement with high-dimensional encoding," New J. Phys. **17**, 022002 (2015).
4. M. Mirhosseini, O. S. Magana-Loaiza, M. N. O. Sullivan, B. Rodenburg, M. Malik, M. P. Lavery, M. J. Padgett, D. J. Gauthier, and R. W. Boyd, "High-dimensional quantum cryptography with twisted light," New J. Phys. **17**, 033033 (2015).
5. I. Ali-Khan, C. J. Broadbent, and J. C. Howell, "Large alphabet quantum key distribution using energy-time entangled bipartite states," Phys. Rev. A **98**, 060503 (2007).
6. M. Kues, C. Reimer, P. Roztocki, L. Romero-Cortes, S. Sciara, B. Wetzel, L. Caspani, J. Azana, and R. Morandotti, "On-chip generation of high-dimensional entangled quantum states and their coherent control," Nature **546**, 622–626 (2017).
7. M. Mirhosseini, O. S. Magana-Loaiza, S. M. Hashemi Rafsanajani, and R. W. Boyd, "Compressive direct measurement of the quantum wave function," Phys. Rev. Lett. **113**, 090402 (2014).
8. S. H. Knarr, D. J. Lum, J. Schneeloch, and J. C. Howell, "Compressive direct imaging of a billion-dimensional optical phase space," Phys. Rev. A **98**, 023854 (2018).
9. M. N. O'Sullivan-Hale, I. A. Khan, R. W. Boyd, and J. C. Howell, "Pixel entanglement: experimental realization of optically entangled d = 3 and d = 6 qudits," Phys. Rev. Lett. **94**, 220501 (2005).
10. L. Martin, D. Mardani, H. E. Kondakci, A. N. Vamivakas, and A. F. Abouraddy, "Basis-neutral Hilbert-space analyzers," Sci. Rep. **7**, 44995 (2017).
11. A. C. Dada, J. Leach, G. S. Buller, M. J. Padgett, and E. Anderson, "Experimental high-dimensional two-photon entanglement and violations of generalized Bell inequalities," Nat. Phys. **7**, 677–680 (2011).
12. J. C. Howell, R. S. Bennink, and R. W. Boyd, "Realization of the Einstein-Podolsky-Rosen paradox using momentum and position-entangled photons from spontaneous parametric down conversion," Phys. Rev. Lett. **92**, 210403 (2004).
13. G. A. Howland and J. C. Howell, "Efficient high dimensional entanglement imaging with a compressive sensing double-pixel camera," Phys. Rev. X **3**, 011013 (2013).
14. D. Giovannini, J. Romero, J. Leach, A. Dudley, A. Forbes, and M. P. Padgett, "Characterization of high-dimensional entangled systems via mutually unbiased measurements," Phys. Rev. Lett. **110**, 143601 (2013).
15. O. Kuzucu, F. N. C. Wong, S. Kurimura, and S. Tovstonog, "Joint temporal density measurements for two-photon state characterization," Phys. Rev. Lett. **101**, 153602 (2008).
16. D. Oren, M. Mutzafi, Y. C. Eldar, and M. Segev, "Quantum state tomography with a single measurement setup," Optica **4**, 993–999 (2017).
17. D. J. Lum, S. H. Knarr, and J. C. Howell, "Fast Hadamard transforms for compressive sensing of joint systems: measurement of a 3.2 million-dimensional bi-photon probability distribution," Opt. Express **23**, 27636–27649 (2015).
18. W. T. Liu, T. Zhang, J. Y. Liu, P. X. Chen, and J. M. Yuan, "Experimental quantum state tomography via compressed sampling," Phys. Rev. Lett. **108**, 170403 (2012).
19. A. Shabani, R. L. Kosut, M. Mohseni, H. Rabitz, M. A. Broome, M. P. Almeida, A. Fedrizzi, and A. G. White, "Efficient measurement of quantum dynamics via compressive sensing," Phys. Rev. Lett. **106**, 100401 (2011).
20. P. Zerom, K. W. C. Chan, J. C. Howell, and R. W. Boyd, "Entangled-photon compressive ghost imaging," Phys. Rev. A **84**, 061804 (2011).
21. O. S. Magana-Loaiza, G. Howland, M. Malik, J. C. Howell, and R. W. Boyd, "Compressive object tracking using entangled photons," Appl. Phys. Lett. **102**, 231104 (2013).
22. N. Uribe-Patarroyo, A. Fraine, D. S. Simon, O. Minaeva, and A. V. Sergienko, "Object identification using correlated orbital angular momentum states," Phys. Rev. Lett. **110**, 043601 (2013).
23. Z. Yang, O. S. Magana-Loaiza, M. Mirhosseini, Y. Zhou, B. Gao, L. Gao, S. M. Hashemi Rafsanjani, G.-L. Long, and R. W. Boyd, "Digital spiral object identification using random light," Light: Sci. Appl. **6**, e17013 (2017).
24. P. A. Morris, R. S. Aspden, F. E. C. Bell, R. W. Boyd, and M. J. Padgett, "Imaging with a small number of photons," Nat. Commun. **6**, 5913 (2015).
25. M. Candes and J. Romberg, "Sparsity and incoherence in compressive sampling," Inverse Probl. **23**, 969–985 (2007).
26. C. Li, W. Yin, H. Jiang, and Y. Zhang, "An efficient augmented Lagrangian method with applications to total variation minimization," Comput. Optim. Appl. **56**, 507–530 (2013).
27. M. Avenhaus, A. Eckstein, P. J. Mosley, and C. Silberhorn, "Fiber-assisted single-photon spectrograph," Opt. Lett. **34**, 2873–2875 (2009).
28. T. Gerrits, F. Marsili, V. B. Verma, L. K. Shalm, M. Shaw, R. P. Mirin, and S. W. Nam, "Spectral correlation measurements at the Hong-Ou-Mandel interference dip," Phys. Rev. A **91**, 013830 (2015).
29. T. Gerrits, M. J. Stevens, B. Baek, B. Calkins, A. Lita, S. Glancy, E. Knill, S. W. Nam, R. P. Mirin, R. H. Hadfield, R. S. Bennink, W. P. Grice, S. Dorenbos, T. Zijlstra, T. Klapwijk, and V. Zwiller, "Generation of degenerate, factorizable, pulsed squeezed light at telecom wavelengths," Opt. Express **19**, 24434–24447 (2011).
30. F. Marsili, V. B. Verma, J. A. Stern, S. Harrington, A. E. Lita, T. Gerrits, I. Vayshenker, B. Baek, and S. W. Nam, "Detecting single infrared photons with 93% system efficiency," Nat. Photonics **7**, 210–214 (2013).
31. G. Harder, T. J. Bartley, A. E. Lita, S. W. Nam, T. Gerrits, and C. Silberhorn, "Single-mode parametric-down-conversion states with 50 photons as a source for mesoscopic quantum optics," Phys. Rev. Lett. **116**, 143601 (2016).

32. S. Etcheverry, G. Canas, E. S. Gomez, W. A. T. Nogueira, C. Saavedra, G. B. Xavier, and G. Lima, "Quantum key distribution session with 16-dimensional photonic states," Sci. Rep. **3**, 2316 (2013).
33. A. Christ, K. Laiho, A. Eckstein, T. Lauckner, P. J. Mosley, and C. Silberhorn, "Spatial modes in waveguided parametric down-conversion," Phys. Rev. A **80**, 033829 (2009).
34. V. Rastogi, K. Thyagarajan, M. R. Shenoy, M. D. Micheli, and D. B. Ostrowsky, "Modeling of large-bandwidth parametric amplification in the Čerenkov-idler configuration in planar waveguides," J. Opt. Soc. Am. B **14**, 3191–3196 (1997).
35. D. H. Auston, "Subpicosecond electro-optic shock waves," Appl. Phys. Lett. **43**, 713–715 (1983).
36. P. Mouroulis and J. Macdonald, *Geometrical Optics Optical Design* (Oxford University, 1997).
37. J. Mallon and P. F. Whelan, "Calibration and removal of lateral chromatic aberration in images," Pattern Recogn. Lett. **28**, 125–135 (2007).
38. J. Roslund, R. M. Araujo, S. Jiang, C. Fabre, and N. Treps, "Wavelength-multiplexed quantum networks with ultrafast frequency combs," Nat. Photonics **8**, 109–112 (2014).